

Noncompact crystalline solids in the square-well potential

Juan Serrano-Illán and Guillermo Navascués*

Departamento de Física Teórica de la Materia Condensada, Universidad Autónoma de Madrid, E-28049 Madrid, Spain

Enrique Velasco

Departamento de Física Teórica de la Materia Condensada and Instituto de Ciencia de Materiales Nicolás Cabrera, Universidad Autónoma de Madrid, E-28049 Madrid, Spain

(Received 21 April 2005; revised manuscript received 25 August 2005; published 26 January 2006)

We reexamine the phase diagram of the square-well potential, using both theoretical and computer-simulation techniques, for not too short ranges of the potential. The phase diagram turns out to contain a variety of crystalline structures, both compact and, interestingly, also noncompact. The latter result from a large increase in negative energy when pairs of particles come at distances within the interaction range, which more than compensates the entropy loss associated with reduced packing. Transitions between these crystalline structures give rise to a surprisingly rich phase diagram.

DOI: [10.1103/PhysRevE.73.011110](https://doi.org/10.1103/PhysRevE.73.011110)

PACS number(s): 64.10.+h, 64.60.-i, 64.70.Kb, 82.70.Dd

I. INTRODUCTION

The square-well (SW) pair potential is a cornerstone of the theory of simple liquids [1], and is still extensively used to study complex systems, from molecular liquids to glasses [2–6], and in other problems such as confinement [7], freezing [8], criticality [9], and more [10–12]. Although not completely realistic, the potential has been used to represent effective interactions in interesting physical systems such as colloids, proteins, alloys, or even water [13–16]. Its phase diagram includes a freezing transition from liquid to a (compact) face-centered cubic (fcc) crystal, along with liquid condensation at low temperature. As the range of the potential $\sigma + \delta$ [where σ is the hard-sphere (HS) diameter] decreases, condensation eventually disappears, while the system undergoes an isostructural transition between two fcc solids of different density [17–19]. The latter occurs when some pairs of neighbors are at distances close to $\sigma + \delta$ so that, in principle, a family of similar transitions should operate associated to nearest, next-nearest, etc., distances. This phase diagram has been confirmed by simulation and theoretical work. In addition, pioneering work by Young [20] and Alder and Young [21] demonstrated that the hexagonal close-packed (hcp) structure may also be stable for $\delta/\sigma > \sqrt{8/3} \approx 0.63$ and that, even more surprising, the body-centered cubic (bcc) structure, a noncompact structure, could be stable for $\delta/\sigma > 2/\sqrt{3} \approx 0.15$; these findings, however, have not been confirmed by computer simulation. In this paper we show that the phase diagram of the SW model may be much more complex than the above picture implies. Using simple arguments, corroborated by sounder theoretical techniques and computer simulations, we find that, not only can the bcc structure be stabilized, but also a variety of other noncompact crystalline phases, provided the potential range is not too short ($\delta \gtrsim 0.15\sigma$). These structures result from a particularly favorable arrangement of pairs of particles that, depend-

ing on the crystalline structure, may come within the interaction range (i.e., within the potential well); this involves a large lowering of the energy which counterbalances the loss of entropy due to these structures being more open, i.e., less compact. Our study was focused to understand a point apparently missed by previous authors. For values of δ such that the fcc-fcc transition is due to next-nearest neighbors, the temperature of the gas-liquid-solid triple point T_{GLS} is higher than that of the gas-fcc-fcc triple point T_{GSS} . But T_{GSS} increases with δ , while T_{GLS} changes by a small amount, so that both should be identical for some δ^* , and a quadruple point should arise [22], a rather unusual situation for one-component systems but quite plausible if the model has an extra degree of freedom [23], in our case δ . The point is that, depending on the approach used for the HS reference system, perturbation theory predicts either the picture described above, with a quadruple point in the phase diagram for a particular value of δ , or the presence of an island of fcc stability in the same region of the phase diagram and in a range of values of δ . The dependence on the chosen reference system is due to the strong sensitivity of the coexistence conditions to small variations in the free energy surface. In the process of elucidating this point by Monte Carlo (MC) simulation, we found that the fcc crystal is not stable in the neighborhood of T_{GLS} and that other, noncompact, crystalline phases become stable.

In Sec. II we propose, using a simple heuristic model, a mechanism which explains the possible stability of different structures. Section III is devoted to a generalization of perturbation theory which aims to describing the Helmholtz free energy of these structures. Due to the complexity brought about by the structural anisotropies, we keep the theory as simple as possible while still including the essential physical features. This theory predicts a complex phase diagram where the fcc structure is not the equilibrium structure in the low-temperature region, as was thought to be the case; in this region a series of different structures appear. To confirm this behavior we present, in both Sec. IV and the Appendix, some MC simulation results obtained using isothermal (NVT) and isobaric (NPT) techniques. The simulation results support the

*Electronic address: guillermo.navascues@uam.es

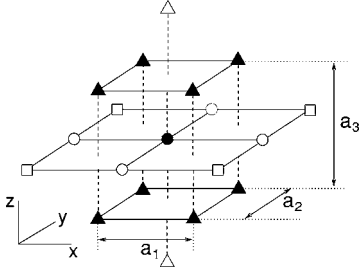


FIG. 1. Generic body-centered tetragonal (ct) structure showing different lattice sites in the neighborhood of a given central site. Sites belonging to the same neighbor shell are indicated by the same symbol.

essential predictions of the theory. Using our theoretical approach and MC simulations we have explored the SW phase diagram for different values of δ . As δ is varied, the stability regions of different structures are reduced or increased, and new structures may appear and others disappear (this behavior has already been observed by Young [20] using a cell model, but restricting attention to a limited number of phases). All results presented here correspond to a specific value of the potential range, namely, $\sigma + \delta = 1.43$. We consider this as a representative case in the sense that it illustrates how the fcc structure is superseded by other structures at the low-temperature region of the phase diagram. There are other (minor) reasons why we choose this specific value of δ , but they will become clear only when we present the final phase diagram. In order to get an idea of the range of this potential, we can integrate the attractive part of a Lennard-Jones potential with the same well depth ϵ and length σ parameters, and compare the result with the corresponding integrated square-well potential; equality is obtained when $\sigma + \delta \approx 1.54\sigma$, which means that the square-well potential that we are about to analyze is not very long ranged at all.

II. SIMPLE HEURISTIC MODEL

In order to understand how crystalline phases become stable, we first provide a heuristic argument based on the number of neighbors—strictly of lattice sites [24]—of a given particle that are inside the well, m , a quantity which will play an essential role. Thus, the isostructural transition involves the phases fcc(12) and fcc(18), with six neighbors coming into (or going out from) the potential well (the number in parentheses is the value of m for the corresponding phase). The question about the identity of the stable phase that supersedes the usual fcc phase can be answered by searching for those structures compact enough to minimize the energy but, at the same time, as symmetric as possible to maximize the entropy. As a first candidate we consider a generic body-centered tetragonal (ct) structure (see Fig. 1) which is stretched or compressed only along one of its edges (by varying a_3 with $a_1 = a_2$), so as not to introduce large anisotropic deformations. This structure may generate a fcc structure when $a_3/a_1 = \sqrt{2}$, but also a bcc structure if $a_3/a_1 = 1$, and a particularly symmetric ct structure [25] (denoted

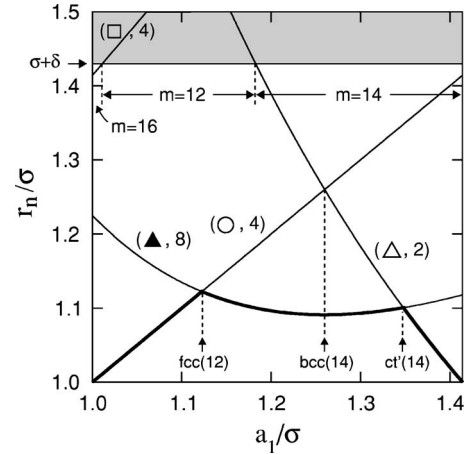


FIG. 2. Distance from a central particle to four successive shells of neighbors versus lattice parameter a_1 for a generic ct structure. The mean number density is $\rho\sigma^3 = 1$. Identity of each shell is indicated by symbols (see Fig. 1), together with its coordination. Thick line gives distance to nearest neighbors. Locations of fcc, bcc, and ct' structures are indicated by an arrow. Shaded region represents radial distances $r \geq \sigma + \delta$, with $\delta = 0.43\sigma$. Values of m in each interval of a_1 are also indicated.

by ct') for $a_3/a_1 = \sqrt{2/3}$. In our search for the more stable structures we found it convenient to work at constant mean number density $\rho = 2/a_1^2 a_3$, so that only one lattice parameter, say a_1 , can be varied. Figure 2 shows the distance r_n of the first four shells of neighbors, $n = 1, \dots, 4$, to a central particle, as a function of a_1 and at reduced density $\rho\sigma^3 = 1$. Note that the behavior of r_n , and hence m , depends very sensitively on both the shell index n and the lattice constant a_1 , and this simple but not regular dependence gives the clue for determining the possible stable structures. From the figure we see that, as a_1 increases from σ to $\sigma\sqrt{2}$, we have $m = 16$ [ct(16) structure], then $m = 12$ [ct(12), including the case fcc(12) for $a_1 = 2^{1/6}\sigma$], and finally $m = 14$ for $1.18\sigma \leq a_1 \leq \sigma\sqrt{2}$ [ct(14), including the cases bcc(14) and ct'(14) for $a_1 \approx 1.26\sigma$ and $a_1 \approx 1.35\sigma$, respectively]. Based on Fig. 2 and using simple arguments one can predict approximately the sequence of stable phases. The entropy can be estimated as a function of a_1 , since it should be approximately proportional to the logarithm of the accessible volume and this is determined essentially by the location of the nearest neighbors, indicated by a thick line in Fig. 2. Thus, the entropy should first increase up to a maximum [fcc(12) structure], then decrease down to the local minimum [bcc(14)], increase again up to the secondary maximum [ct'(14)], and finally decrease; this behavior agrees with the predictions of a more sophisticated model (see Sec. III). Note that all structures have a lower entropy than the fcc(12) structure; however, in the interval $1.18 \leq a_1/\sigma \leq \sqrt{2}$ the ct(14) structure has two additional neighbors in the well which lowers energy but also entropy. In order to discriminate between these structures with 14 neighbors, we go a little further and propose an additional condition: to maximize the energy decrease, the additional particles (which can be two or four, apart from the main set of eight) should be well inside the attractive well, i.e., the distance of their lattice sites—equilibrium

positions—to the boundary of the potential well must be at least equal to the root mean square deviation of the corresponding particles, roughly estimated as the nearest-neighbor distance minus σ . This argument excludes the lower values of a_1 in the interval $1.18 \leq a_1/\sigma \leq \sqrt{2}$, corresponding to two additional particles, and also the higher values, where four particles are too close to the boundary of the well. Thus possible stable structures are reduced to a small region around bcc(14), which is remarkable as it suggests that a typical noncompact structure in systems with soft repulsive interactions can also be stable for the SW model, an attractive model with hard-core interactions. Note that the ct(16) structure, with values of a_1 very close to σ , should also be excluded except at sufficiently low temperatures, because despite having $m=16$, four of them are not deep inside the well and its low entropy cannot be counterbalanced by energy. Doing the same analysis at different densities we arrive at the following sequence of possible stable crystalline structures, from low density to close packing: bcc(14)-ct'(14)-ct(14)-fcc(18). Naturally, when the temperature is high enough only the fcc crystal will be stable.

III. A PERTURBATION THEORY

Thus far the discussion has focused on a plausible mechanism that might induce the stabilization of noncompact structures. To confirm the above conjectures we have formulated a simple perturbation theory, complemented with MC simulations to be presented in Sec. IV. The theory is based on a generalization of the free-volume approach for the entropy of the HS solid [26] that takes account of the structural anisotropies of the crystal and, in the same spirit, of the corresponding generalization of the angular-averaged HS distribution function [27]. The theory also introduces an *ad hoc* model to incorporate the geometry of the different structures. The Helmholtz free energy expression for the SW model, up to first order, is given exactly by [28]

$$\frac{\beta F}{V} = \frac{\beta F_{\text{HS}}}{V} - 2\pi\rho^2\epsilon \int_{\sigma}^{\sigma+\delta} dr r^2 \tilde{g}_{\text{HS}}(r), \quad (1)$$

where F_{HS} and $\tilde{g}_{\text{HS}}(r)$ are the Helmholtz free energy and the angular-averaged distribution function of the HS reference system, respectively, V is the volume, and $\beta=1/kT$. For the liquid phase the HS free energy was taken to be given by the Carnahan-Starling [29] expression, whereas the function $\tilde{g}_{\text{HS}}(r)$, which in this case reduces to the usual radial distribution function, was approximated by the Verlet-Weis expression [30]. The free-volume expression for the Helmholtz free energy of the crystal is

$$\frac{\beta F_{\text{HS}}}{V} = -\rho \ln \frac{v(\rho)}{\Lambda^3}, \quad (2)$$

where $v(\rho)$ is the free volume (i.e., the volume available to a given sphere assuming all the neighbor spheres are fixed at their equilibrium sites), and Λ the thermal wavelength. The analytic expression for the free volume can be obtained exactly for a given crystallographic structure, but only after some laborious analytical work (especially if the structure

does not possess a high symmetry). For simplicity we have chosen to evaluate the free volume by MC integration in all the structures analyzed. The second ingredient of the theory is the function $\tilde{g}_{\text{HS}}(r)$. For the fcc phase all the peaks of this function, except the first, are very accurately given by the convolution of the local density $\rho(\mathbf{r})$. To be more precise, simulation results show that there is no significant numerical difference between the peaks of the function $\tilde{g}_{\text{HS}}(r)$ and those obtained from the convolution of $\rho(\mathbf{r})$. This means that the essential correlations in ordered phases are somehow extended up to relatively short distances, maybe including next-nearest neighbors. We will assume in what follows that this is the case in all structures formed out of hard spheres; in fact, the results to be presented later show that this assumption should hold or at least be very accurate. Thus we approximate the angular-averaged distribution function, at distances beyond nearest neighbors, by

$$\begin{aligned} \tilde{g}_{\text{HS}}(r) &\equiv \frac{1}{4\pi V \rho^2} \int d\mathbf{r}' \int d\hat{\Omega} \rho^{(2)}(\mathbf{r} + \mathbf{r}', \mathbf{r}') \\ &\approx \frac{1}{4\pi V \rho^2} \int d\mathbf{r}' \int d\hat{\Omega} \rho(\mathbf{r} + \mathbf{r}') \rho(\mathbf{r}'), \end{aligned} \quad (3)$$

where $\rho^{(2)}(\mathbf{r}, \mathbf{r}')$ is the two-body distribution function, and $d\hat{\Omega}$ is the solid-angle differential. Now the first peak generated by this expression and corresponding to the nearest neighbors must be modified so that it exhibits a correlation hole of range σ [which is realized in practice by simply setting $\tilde{g}_{\text{HS}}(r)$ to zero for $r \leq \sigma$]. Also, the first peak has to be renormalized so as to give the correct number of nearest neighbors (in fact a renormalization of the second peak is also necessary at densities low enough that the peak extends to distances less than σ). A more accurate approximation for this peak could be made (for example, by generalizing the self-consistent theory recently proposed by some of us [31]) but in the present case this is actually unnecessary since the peak lies completely inside the potential well and consequently contributes with a constant value (equal to the number of nearest neighbors multiplied by $\epsilon/2$) to the free energy, regardless of its functional form (this also applies to the second peak for phases such that at low density the peak is completely inside the well). Taking this fact into account, the problem of finding $\tilde{g}_{\text{HS}}(r)$ reduces to obtaining the local density $\rho(\mathbf{r})$, defined as

$$\rho(\mathbf{r}) = \sum_i \rho_1(\mathbf{r} - \mathbf{R}_i), \quad (4)$$

where $\rho_1(\mathbf{r} - \mathbf{R}_i)$ is the distribution function of the i th particle about its equilibrium position, given by the lattice vector \mathbf{R}_i . An interesting feature of the present study is that some of the phases we are dealing with do not have cubic symmetry, and consequently their corresponding function $\rho_1(\mathbf{r})$ cannot be approximated by a spherically symmetric Gaussian function, as in the case of the fcc phase or (to a lesser extent) the bcc phase. Thus, in order to incorporate the local anisotropy, we propose a normalized Gaussian with a general quadratic form as argument:

$$\rho_1(\mathbf{r}) = \sqrt{\frac{\alpha_x \alpha_y \alpha_z}{\pi^3}} e^{-(\alpha_x x^2 + \alpha_y y^2 + \alpha_z z^2)}. \quad (5)$$

To determine the Gaussian parameters we impose three conditions. The first is a generalization of our free-volume approach for cubic structures; in that case $\alpha_x = \alpha_y = \alpha_z = \alpha$, and the free volume is identified with the spherical volume determined from $r_{\text{rms}} \equiv \langle r^2 \rangle^{1/2}$ (the root mean-square displacement [26]):

$$v = \frac{4\pi}{3} \langle r_{\text{rms}}^2 \rangle^{3/2} = \frac{4\pi}{3} \left(\frac{3}{2\alpha} \right)^{3/2}. \quad (6)$$

A direct generalization to the general anisotropic case gives

$$v = \frac{4\pi}{3} \left(\frac{3}{2\alpha_x} \right)^{1/2} \left(\frac{3}{2\alpha_y} \right)^{1/2} \left(\frac{3}{2\alpha_z} \right)^{1/2}. \quad (7)$$

Note that Eq. (7) corresponds to the volume of an ellipsoid with semiaxes $(3/2\alpha_x)^{1/2}$, $(3/2\alpha_y)^{1/2}$, and $(3/2\alpha_z)^{1/2}$. For the (cubic) fcc structure this simple approach gives numerical results remarkably similar to those found using density-functional theories, which are computationally more demanding. Also, reasonable results are obtained for the bcc phase, for which density-functional theory generates unphysical results [26]. In the general, anisotropic case, the volume itself is unable to characterize the anisotropy, so two additional conditions are required. A natural choice is to relate the Gaussian parameters to the particle mean-square displacements $\langle x^2 \rangle$, $\langle y^2 \rangle$, and $\langle z^2 \rangle$ along the x , y , and z , directions, respectively, which can be obtained independently by some numerical means. The relations are

$$\frac{\langle x^2 \rangle}{\langle z^2 \rangle} = \frac{1/\alpha_x}{1/\alpha_z} \quad (8)$$

together with

$$\frac{\langle y^2 \rangle}{\langle z^2 \rangle} = \frac{1/\alpha_y}{1/\alpha_z}. \quad (9)$$

In what follows it is to be understood that these thermal averages have been obtained via Monte Carlo integration, i.e., $\langle \cdots \rangle = \langle \cdots \rangle_{\text{MC}}$, in much the same way as the free volume $v(\rho)$ in Eq. (2) will be assumed to have been computed using numerical integration. Note that several equivalent prescriptions to describe the anisotropy are possible. Obviously, for cubic structures, $\langle x^2 \rangle = \langle y^2 \rangle = \langle z^2 \rangle$, and the three Gaussian parameters are identical. In almost all cases to be studied in the present work there are at least two equivalent directions, say x and y , so that $\alpha_x = \alpha_y$, which, for the sake of simplicity, we rename as α (we must say that phases with $\alpha_x \neq \alpha_y$ have been analyzed in the present work, but the corresponding anisotropic structures always happen to be metastable). In these cases the conditions (7), (8), and (9) reduce to

$$v = \frac{4\pi}{3} \frac{3}{2\alpha} \left(\frac{3}{2\alpha_z} \right)^{1/2} \quad (10)$$

and

$$\frac{\langle x^2 \rangle}{\langle z^2 \rangle} = \frac{1/\alpha}{1/\alpha_z}. \quad (11)$$

In principle, as v , $\langle x^2 \rangle$, $\langle y^2 \rangle$, and $\langle z^2 \rangle$, which clearly depend on the lattice parameters a_1 , a_2 , and a_3 , are known from MC integration, one could evaluate the Gaussian parameters α and α_z directly. However, we must bear in mind that the relation $\rho = \rho(a_1, a_2, a_3)$ for the mean density still leaves two independent ways in which the unit cell can be deformed, so that additional conditions are required. Here we introduce an *ad hoc* geometrical model, inspired by the heuristic model introduced in the previous section, which is very simple for phases with $a_1 = a_2$ and slightly more complicated in the general case. Here we restrict ourselves to the former, simpler case, where $a_1 = a_2$ and the relation $\rho = \rho(a_1, a_3)$ leaves only one independent lattice parameter (say a_1), and therefore only one additional relation is needed. The idea behind the model is straightforward: in order to minimize the free energy, we optimize the structure of the unit cell by increasing the free volume available to a central sphere (so as to maximize entropy) while at the same time the energy contribution is maximized. The optimization of the structure is realized in practice by applying an appropriate, volume-conserving, anisotropic deformation to the unit cell, with the property that the shell of neighbors of the central sphere (henceforth called *boundary spheres*) closest to the boundary of the well (which is located at $r = \sigma + \delta$) is *completely* inside the potential well. In practical terms, *completely* means that the distance of the boundary spheres to the boundary of the well is taken to be equal to the semiaxes $(3/2\alpha_i)^{1/2}$, where $i = x, y$, or z (depending on the direction along which the neighbors are arranged), so that most of the time (or, more precisely, in most of the possible particle configurations) these spheres are inside the potential well. The condition leads to

$$\sigma + \delta = d + \left(\frac{3}{2\alpha_i} \right)^{1/2}, \quad (12)$$

where d is the distance from the central sphere to the boundary spheres (which also depends on the type of structure). For instance, for a generic ct(14) phase (obtained, say, when $a_1/\sigma = 1.2$), the ellipsoid associated with the Gaussian functions of the two boundary spheres (open triangles in Figs. 1 and 2), which lie along the z direction, can be easily seen to have a symmetry axis parallel to the radial direction. Moreover, as seen from Fig. 1, $d = a_3$, and the condition reads

$$\sigma + \delta = a_3 + \left(\frac{3}{2\alpha_z} \right)^{1/2}. \quad (13)$$

In the case of the ct(16) phase (take a_1 slightly larger than σ ; see Fig. 1), the symmetry axis of the corresponding Gaussian functions points in the z direction and is therefore perpendicular to the radial direction (the boundary spheres are on the xy plane; open squares in Figs. 1 and 2). In this case $d = a_1\sqrt{2}$, and

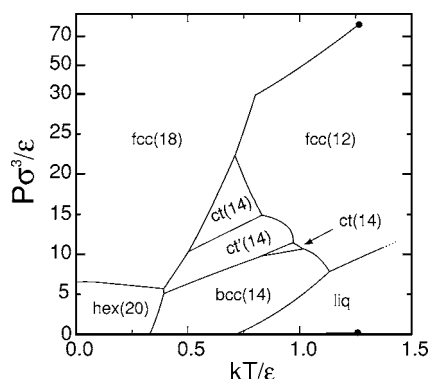


FIG. 3. Phase diagram for the square-well model with $\delta = 0.43\sigma$ in the reduced pressure–reduced temperature plane, as obtained from the perturbation theory proposed in the text. Kink in fcc(18)-fcc(12) transition line is due to a change in the pressure scale. Lines indicate first-order phase boundaries. Circles are critical points. Dots indicate that phase boundary continues indefinitely. See text for an explanation of labels.

$$\sigma + \delta = a_1 \sqrt{2} + \left(\frac{3}{2\alpha}\right)^{1/2}. \quad (14)$$

In summary, solving for each structure Eqs. (10)–(12) simultaneously, along with the expression for the mean density $\rho = \rho(a_1, a_3)$, we can obtain an approximation for $\tilde{g}_{\text{HS}}(\mathbf{r})$. With this approximation and Eq. (2) the Helmholtz free energy can be evaluated directly via perturbation theory, Eq. (1). The same procedure can be repeated for all phases. Note that in the case of phases, such as the cubic phases or the ct'(14) phase, for which the density already determines the lattice parameters in a unique way, the optimization of the structure is not necessary. More involved calculations, based on more sophisticated approaches, could be carried out. Besides the above-mentioned self-consistent evaluation of F_{HS} and $\tilde{g}_{\text{HS}}(r)$, one could introduce some minimization principle, for instance instead of fixing the position of the boundary spheres following the criterion implicit in Eq. (12), we could minimize the free energy with respect to this position. Alternatively we could minimize the free energy with respect to the Gaussian parameters. However, these improvements would complicate the calculations significantly and, since we have already developed a simple procedure that should contain the essential physics of the problem, we will not implement any of these more involved approaches. The above theory has been applied to the fcc, bcc, ct'(14), ct(14), and ct(16) phases, and also to the hexagonal [hex(20)] structure (with $a_1 = a_2 \neq a_3$), which contains 20 particles inside the well [32]. Furthermore we have studied the simple cubic (sc) and some simple monoclinic structures obtained by applying relatively symmetric deformations (e.g., shearing) to the ct phase. None of these become thermodynamically stable, though they are metastable in some range of temperatures and densities. We will not discuss these phases any further, but it is interesting to mention that these phases, albeit metastable, do appear in the computer simulations, possibly as transient or nonequilibrium phases. The phase diagram obtained is shown in Fig. 3. As can be seen the theoretical

predictions basically agree with our previous conjectures based on the simple heuristic model, even as far as the relative stability of the phases is concerned.

IV. COMPUTER SIMULATION

To corroborate this complex phase diagram extensive MC simulations were conducted on systems with $N \sim 10^2 - 10^3$ particles, using constant-volume (*NVT*) and constant-pressure (*NPT*) runs and typically $(0.5 - 1) \times 10^5$ MC steps. In *NVT* simulations the box sides were allowed to fluctuate with the restriction $V = \text{const}$, so that the system could better accommodate different crystal deformations without accumulating any anisotropic stresses. In fact, during the simulations the box lengths fluctuate about a (constant) average value, which we assume to indicate a situation of equilibrium. Also, average positions of the particles were monitored during the simulations in order to see whether groups of particles could be escaping from their cages, or crystallographic planes could slide with respect to each other. This information is similar to that gathered by computing elastic constants, which would give a clear indication as to the mechanical stability of the different structures, but is a major task to accomplish (given the discontinuous nature of the potential) and will not be pursued here. Note also that no attempt was made to evaluate the free energy by computer simulation, except for the vapor, liquid, fcc, and hex phases, for which thermodynamic integration schemes can be designed and their corresponding coexistence lines computed rigorously. One obvious limitation of the above simulation techniques is that the number of particles N is fixed, so that we have to impose a given structure at the beginning (grand canonical Monte Carlo simulation is impractical for crystalline solids) and hope that the structure is stable. In most cases the system undergoes a transition to a different crystalline structure with the same number of particles per unit cell, so that the above techniques can in fact reach the equilibrium phase by way of deforming the unit cell. This is not always the case, and parameters such as number of particles (among the set of possible values for the given structure) and technique used (*NVT* or *NPT*) affect the final outcome of the simulation. This is not a problem since, in all cases, an equilibrated state is easily detected by monitoring the evolution of box lengths and average positions; when these criteria were not met, the final configuration was rejected. (In the Appendix we include some details of simulations which explicitly demonstrate the instability of the fcc phase over a large region of the phase diagram. Finite-size effects on the bcc(14), ct(14), and hex(20) phases are also included in the Appendix.) The results are contained in Fig. 4. The fcc(18)-fcc(12), hex(20)-fcc(18), fcc(12)-liq, and liq-vap phase transitions thus located are indicated by continuous lines. The remaining, dotted lines correspond to approximate location of phase transitions, based on *NVT* and *NPT* simulations (in some cases particles in the simulation box simply adopt a new periodic arrangement on changing thermodynamic conditions; in other cases instabilities are signaled by deformations of layers of particles or the unit cell). These lines indicate approximately the average of the two points marking the

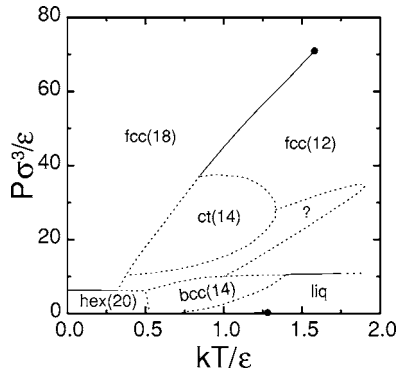


FIG. 4. Same as in Fig. 3 but as obtained from Monte Carlo simulation. Dotted lines represent approximate phase boundaries as follow from NVT and NPT Monte Carlo simulations. Continuous lines are first-order coexistence lines obtained from free-energy calculations.

end of metastability of each of the two phases that coexist. In the region labeled with “?” we found it difficult to obtain the stable structure since the system does not seem to reach equilibrium. In any case these simulations can only provide at most limits of stability, and the results are only indicative of the possible thermodynamic phase coexistence. However, the simulations undoubtedly indicate that the fcc phase is unstable over a large region of the phase diagram, and that some of the noncompact phases obtained by the theory are at least metastable and good candidates for stable phases. Note also that the region where these phases appear to exist, according to simulation, is considerably larger than predicted by theory.

V. DISCUSSION

To appreciate in more detail the predictive power of the theory we have analyzed the results along the isotherm $T = 0.7\epsilon/k$ since it crosses a number of different phases. In Fig. 5 the theoretical Helmholtz free energies for this isotherm are shown in a particular range of densities. For the sake of clarity we do not include the sc, hex(20), and simple mono-

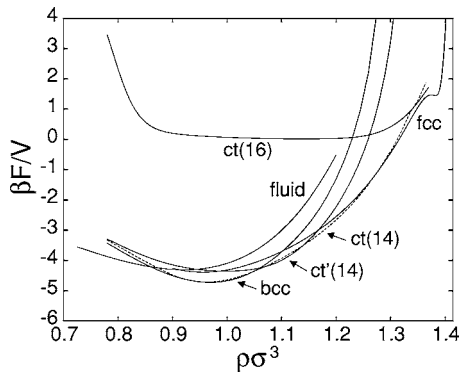


FIG. 5. Helmholtz free energy per unit volume versus reduced density for the square-well model with $\delta=0.43$ at temperature $T = 0.7\epsilon/k$ and for different phases. All results have been obtained from perturbation theory.

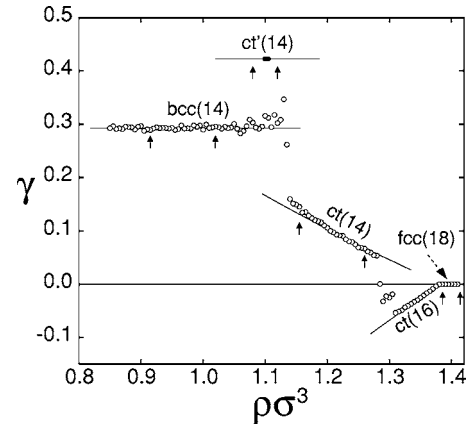


FIG. 6. Order parameter γ versus reduced density $\rho\sigma^3$ at temperature $T=0.7\epsilon/k$ for different phases of the square-well model with $\delta=0.43\sigma$. Continuous lines, perturbation theory. Open circles, computer simulations. Filled circles, simulation runs of the $ct'(14)$ structure with a fixed simulation box. Arrows indicate limits defining density intervals where the corresponding phase is predicted to be stable according to perturbation theory.

clinic structures mentioned above. All of these structures are metastable in a small range of densities. However, the $ct(16)$ phase, which is also metastable, is included for reasons that will become clear later. We define an order parameter γ as

$$\gamma = 1 - \frac{a_3}{a_1\sqrt{2}} \quad (15)$$

which describes the anisotropy of the phases with $a_1=a_2$ and discriminates between different phases with the same symmetry; the presence of the factor $\sqrt{2}$ ensures that $\gamma=0$ for the fcc phase. Note that Eq. (8) could also be adopted as an order parameter; however, this parameter is less sensitive to anisotropy and, in particular, it does not discriminate between the fcc and bcc phases since in the two cases $\langle x^2 \rangle / \langle z^2 \rangle = 1$. For the cubic phases fcc and bcc, γ has density-independent values, viz., 0 and $1 - 1/\sqrt{2}$, respectively, and also for the anisotropic phase $ct'(14)$ for which $\gamma = 1 - 1/\sqrt{3}$ (see Sec. II). For the remaining phases γ depends on the density. In Figs. 6–8 we compare the theoretical predictions for the order parameter and the angular-averaged distribution function along the isotherm $T=0.7\epsilon/k$ with the corresponding results obtained by simulation using the NVT ensemble. This simulation starts from a fcc(18) structure and proceeds by successive expansions, allowing for fluctuations of the sides of the simulation box. In this way we can reach any tetragonal structure and avoid the unknown nontetragonal phase mentioned above. Figure 6 shows the order parameter γ . In general terms the theory agrees reasonably with the simulations. Let us be more specific and discuss these results in connection with Figs. 3 and 5. At high density ($\rho\sigma^3 \approx \sqrt{2}$) the stable phase is a fcc(18) phase. As the system is expanded at constant temperature the parameter γ continues to be zero, but at some density the fcc(18) phase becomes unstable, and γ takes a nonzero value. This can also be seen by examining the particle configurations in the simulations. As can be seen in the figure the order parameter indicates that the system adopts a

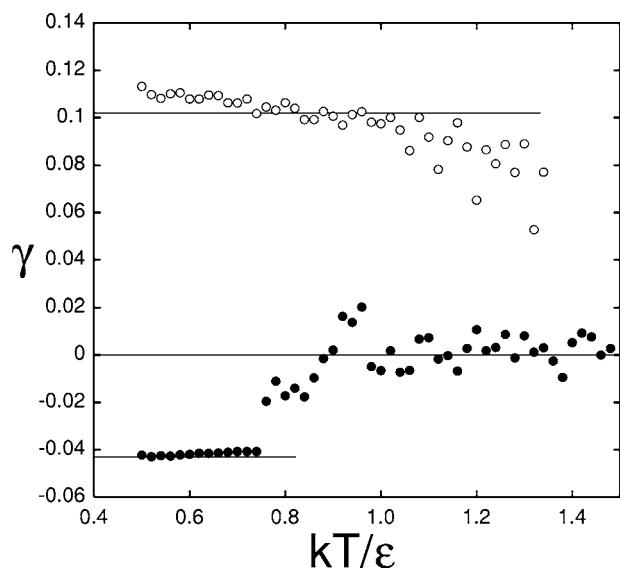


FIG. 7. Behavior of the order parameter γ with reduced temperature kT/ϵ for the square-well model with $\delta=0.43\sigma$. Open circles are simulation results starting from a ct(14) phase at reduced density $\rho\sigma^3=1.20$. Solid circles are simulation results starting from a ct(16) phase with reduced density $\rho\sigma^3=1.33$. Continuous lines are constant values predicted by perturbation theory.

ct(16) structure; this is at variance with the theory which, as suggested by the phase diagram of Fig. 3, predicts coexistence between the fcc(18) and the ct(14) phases. Note however that, as shown in Fig. 5, the theoretical free energies of the ct(14) and ct(16) phases are very similar in this range of

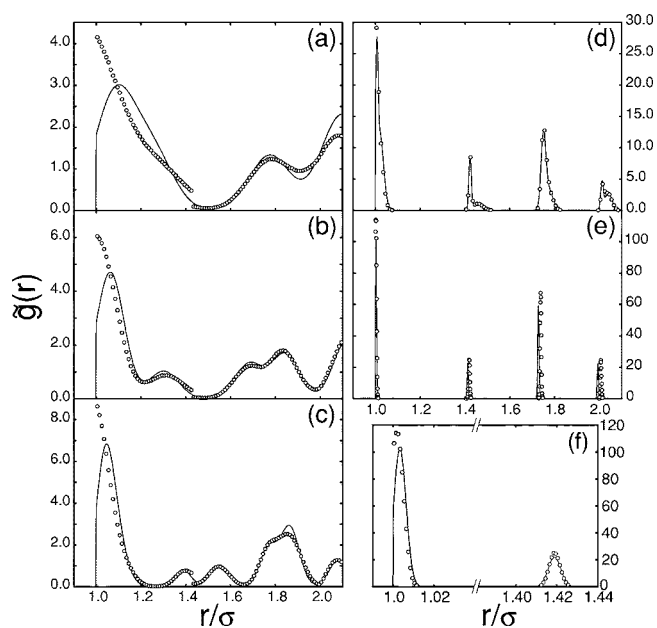


FIG. 8. Angular-averaged distribution function for the HS model as obtained by theory (continuous line) and for the square-well model with $\delta=0.43\sigma$ as obtained by simulation (circles), both at reduced temperature $T=0.7\epsilon/k$. (a) bcc phase with reduced density $\rho\sigma^3=1.00$; (b) ct'(14) phase with $\rho\sigma^3=1.10$; (c) ct(14) phase with $\rho\sigma^3=1.20$; (d) ct(16) phase with $\rho\sigma^3=1.35$; (e) and (f) fcc(18) phase with $\rho\sigma^3=1.40$.

densities, and also that *NPT* simulations show that the ct(16) phase is metastable with respect to direct coexistence between the ct(14) and fcc(18) phases. Then, since the simulation procedure allows for fluctuations in the sidelengths of the simulation box, the system could very well be exploring phases with different symmetries but very similar free energies and connected by a small free-energy barrier. In any case the theoretical predictions on the value of γ for the ct(16) phase are confirmed by simulation. The system remains in the ct(16) phase in a range of densities but, at $\rho\sigma^3 \approx 1.3$, the free energy of this phase becomes much higher than that of the ct(14) or fcc phases (see Fig. 5), and γ fluctuates, indicating that the system enters a region of two-phase coexistence. At lower densities, $\rho\sigma^3 \approx 1.28$, the order parameter follows the theoretical predictions for the ct(14) phase. As we continue to expand, the system goes directly to the bcc(14) phase after crossing a relative large region of instability, a region that was analyzed in the previous section. This is again in disagreement with the theory, which predicts stability in an intermediate ct'(14) phase. As it turns out it is possible to stabilize the ct'(14) phase in the simulation, but only by imposing the appropriate crystal-line structure with a suitable simulation box with fixed side lengths. In this case the resulting values for the order parameter will necessarily agree with the theoretical predictions. Note that the order parameter γ is independent of temperature since it is defined in terms of the lattice parameters which, in perturbation theory, only depend on the (athermal) HS reference system. This is essentially true, as the simulation results demonstrate. In Fig. 7 we show the behavior of γ with temperature for the ct(14) and ct(16) phases at two particular densities. As can be seen, γ changes significantly with density but, in the ct(16) phase, it hardly differs from the constant behavior predicted by the theory at fixed density, and it exhibits only a small decrease in the case of the ct(14) phase. In Fig. 8 we show the function $\tilde{g}_{\text{HS}}(r)$ for the different stable phases, as predicted by theory, along the isotherm $T=0.7\epsilon/k$ (each phase is shown at a different density). The same function at the same temperature and for a density corresponding to the ct(16) phase is also shown. For the sake of comparison, we also include the function $\tilde{g}_{\text{SW}}(r)$ as obtained by computer simulation for the same phases and at the same conditions of density and temperature. Despite being different functions in nature, the reference function $\tilde{g}_{\text{HS}}(r)$ is the zeroth-order approximation to $\tilde{g}_{\text{SW}}(r)$ in perturbation theory, so that the comparison can help to grasp the accuracy of the theory and also the essential structural properties of the phases. One should remember that, provided that the first peak is normalized to the number of nearest neighbors, all the results are insensitive to the functional form adopted so that we should guarantee only the normalization. Also note that the function $\tilde{g}_{\text{HS}}(r)$ is indeed a reasonable approximation to $\tilde{g}_{\text{SW}}(r)$ for all the phases. However, the most significant conclusion we can draw from these results is that, despite its simplicity, the theory is capable of describing the anisotropy. The peaks of the radial distribution function have approximately the same width, except in the ct(16) phase where there are both narrow and relatively sharp peaks, sometimes close to each other. To understand this let us focus on the

third and fourth peaks which, at the chosen density, are located at each side of the SW discontinuity. The distribution functions $\rho_1(\mathbf{r})$ corresponding to the third and fourth peaks are such that their associated Gaussian functions have a semimajor axis perpendicular (open squares in Fig. 1) and parallel (open triangles) to the radial direction, respectively (remember that their Gaussian parameters are related to the axes of the ellipsoid). Since the anisotropy of the Gaussian functions of the ct(14) and ct'(14) phases is not very high, its effect on \tilde{g} is not very apparent. The hexagonal structure, which together with the fcc(18) and a rarified vapor phase, remains stable up to $T=0$, is a clear example that stability depends very sensitively on δ . When δ is slightly less than 0.43σ , the structure disappears altogether from the phase diagram, allowing for the possibility that the previously discarded ct(16) structure may become stable at sufficiently low temperatures [at very low temperatures though, a simple cubic sc(18) structure would be more stable, with direct transitions to vapor and fcc(18) phases]. On the other hand, for $\delta > 0.43\sigma$ the hex(20) structure would significantly increase its stability. As a general rule, an increase in δ entails a considerably larger number of possible stable structures, probably with relatively small deformations. For example, for $\sigma + \delta > 1.63\sigma$, an argument based on results similar to those shown in Fig. 2, together with computer simulations, indicates that the hcp structure becomes stable at densities where the high-density fcc(18) structure would otherwise be stable. These results for the bcc and hcp phases basically agree with those found by Young [20] using a spherical Lennard-Jones-Devonshire-cell approach. However, aside from these phases, Young only considered the sc phase, and found it not to be stable, which is at variance with our results. Later Alder and Young [21], using an extended first-order perturbation theory with averaged quantities over the reference HS evaluated via simulation, did find a stable hcp phase. After the above discussion, we can return to the question as to why the particular value 1.43σ was chosen for $\sigma + \delta$. First of all it should be clear that our basic aim is to show that, at low temperatures, phases with a structure different from the fcc structure are the equilibrium phases for the SW model with a potential range larger than approximately $\delta + \sigma > \approx 1.15\sigma$. Then, in principle, any value of $\sigma + \delta$ that satisfies this criterion could be used for our purposes. It is well known that the fcc(14)-fcc(18) isostructural transition appears at close packing when $\sigma + \delta = \sqrt{2}\sigma$; for larger values of $\sigma + \delta$ this transition moves at lower densities. Therefore for our chosen value, $\sigma + \delta = 1.43\sigma$, this transition is located at very high density which leaves a large region of the phase diagram corresponding to solid stability available for exploring the possible stability of other structures. At larger values of $\sigma + \delta$ the number of candidate stable structures increases and the fcc(14)-fcc(18) isostructural transition moves to lower densities; in principle, both circumstances make the phase diagram more complex and interesting to investigate but at the same time the analysis is much more difficult. On the opposite side, for $\sigma + \delta < \sqrt{2}\sigma$, the phase diagram is free from the fcc(14)-fcc(18) transition, the number of candidate stable structures decreasing, and the phase diagram is expected to be simpler and easier to study. As a compromise, we make the theoretical analysis and do MC

simulations for an intermediate value close to $\sqrt{2}\sigma$, namely $\sigma + \delta = 1.43\sigma$, which includes the fcc(14)-fcc(18) transition at high densities and also the hexagonal phase. For $\sigma + \delta = 1.42\sigma$ the diagram is quite similar to that of Figs. 3 and 4, but without the presence of the hexagonal phase; for a value of 1.41 the fcc(14)-fcc(18) transition is also absent.

VI. SUMMARY AND CONCLUSIONS

In summary, we have shown that the phase diagram of the SW model may be much more complex than previously believed. Remarkably, it seems to have at least three stable noncompact structures; these structures would otherwise be unstable, given that the potential contains a hard core, but in this case they are stabilized by the attractive part of the potential. The results correspond to a particular range of the potential δ , which we believe is representative for the complex character of the phase diagram in general. However, we have evidence that different values of δ , even very close to the value used here, give rise to dramatically different topologies of the phase boundaries. Also, values as low as 0.15σ should give rise to a stable bcc phase with respect to the fcc; however this phase, although mechanically stable, could very well become thermodynamically metastable with respect to other structures [33]. The physical mechanism behind the stabilization of noncompact structures is, as usual, the balance between energy and entropy, which in this case amounts to counting the number of particles that can accommodate within the potential range with an optimized free volume. As δ is increased the number of structures in the phase diagram greatly increases. A simple analysis based on a graph similar to that in Fig. 2 should provide a rough, first estimate as to possible stable phases, and a more elaborate first-order perturbation theory may refine these predictions. Clearly the stability of the noncompact structures will depend on the slope of the attractive part so that, as the potential becomes less abrupt, some phases may lose their stability. The mechanism discussed here should also operate when the pair potential exhibits the oscillatory behavior typical of metallic interactions.

ACKNOWLEDGMENTS

This work has been partially financed by the Ministry of Science and Technology of Spain (Grant No. BFM2001-0224-C02-01).

APPENDIX

In this appendix we present some details of the results obtained from two series of *NPT* simulations for three state points (T, P) on the phase diagram (Fig. 4) where the phases bcc(14), ct(14), and hex(20) seem to be at least metastable. The reduced temperatures kT/ϵ and pressures $P\sigma^3/\epsilon$ of these state points are (0.70, 4.00), (0.90, 28.00), and (0.10, 50.00), respectively. The purpose of these runs is to check whether the stability of these structures is robust with respect to system size and length of the simulations. In the first series of *NPT* simulations we start the system in a perfect fcc configura-

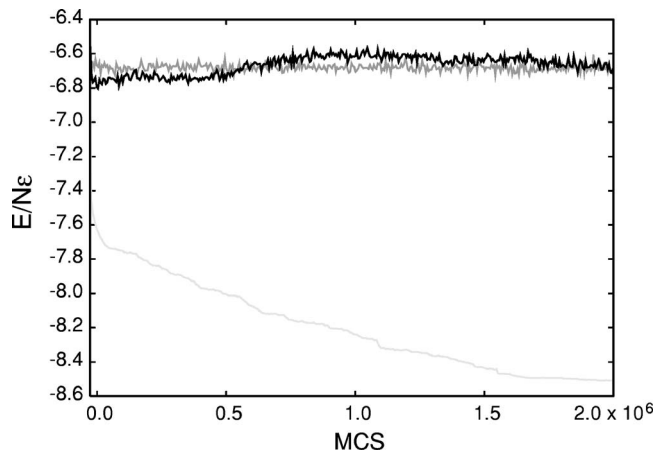


FIG. 9. Evolution of the reduced energy per particle with MC steps (plotted every 2000 steps) for an *NPT* simulation of the square-well model with $\delta=0.43\sigma$ and with an initial fcc configuration. $N=1008$ particles. Black line, $T=0.7\epsilon/k$ and $p\sigma^3/\epsilon=4$; dark gray line, $T=0.9\epsilon/k$ and $p\sigma^3/\epsilon=28$; and light gray line, $T=0.1\epsilon/k$ and $p\sigma^3/\epsilon=5$.

ration with 1008 particles; the simulation box sides are allowed to fluctuate without any change in their orientations. In Figs. 9 and 10 we show the evolution of the reduced energy per particle, $E/N\epsilon$, and the order parameter, γ , with respect to MC steps (data points are plotted every 2000 steps). The order parameter γ was defined in an *ad hoc* manner in order to distinguish between different tetragonal structures. For the sake of completeness, a corresponding order parameter $\gamma' = 1 - a_1/a_3$ has also been defined for the hex(20) phase (and a corresponding figure included) such that it is zero at hexagonal close packing. The instability of the fcc phase is evident in the three cases; note that departure from the fcc configuration occurs rather quickly. This is more easily recognized from the behavior of the order parameter, since the reduced energy per particle of the fcc structure does not differ very substantially from that of the bcc and ct structures. Note also that the system appears to be tending to the

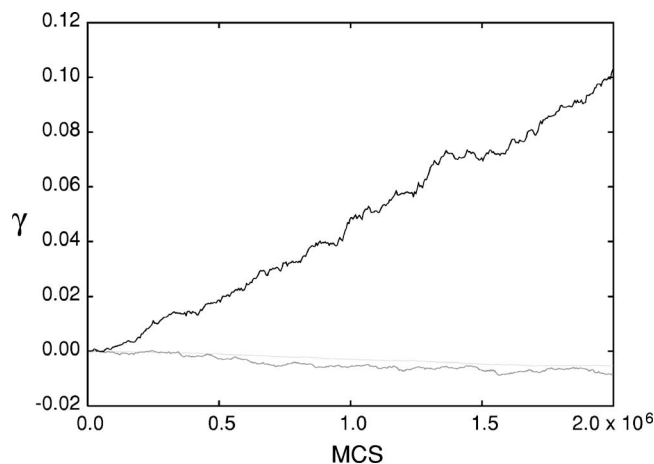


FIG. 10. Evolution of the order parameter γ with MC steps (plotted every 2000 steps) for an *NPT* simulation of the square-well model with $\delta=0.43\sigma$ and with an initial fcc configuration. $N=1008$ particles. Key to lines as in Fig. 9.

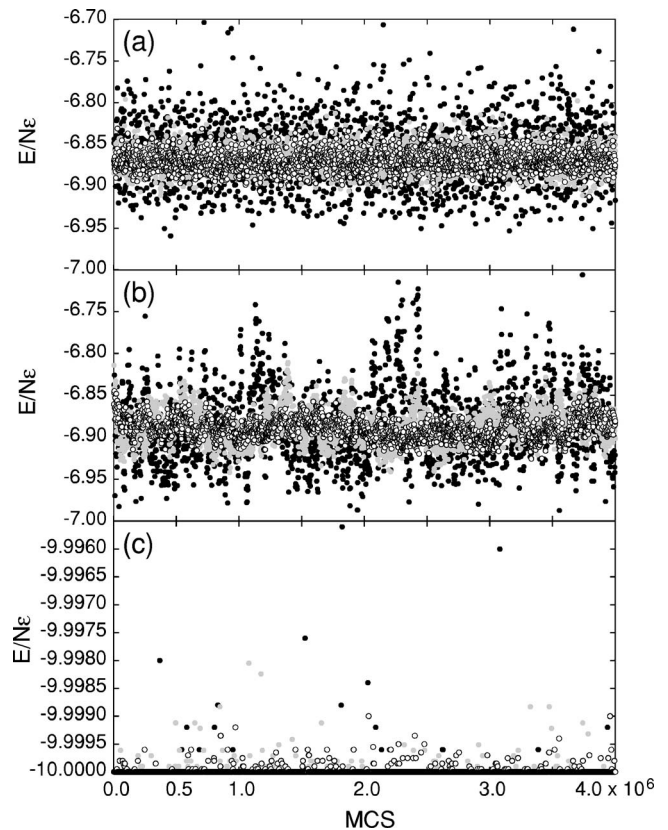


FIG. 11. Evolution of the reduced energy per particle with MC steps (MCS), plotted every 4000 steps, for an *NPT* simulation of the square-well model with $\delta=0.43\sigma$. (a) Initial configuration is bcc structure. Reduced temperature is $kT/\epsilon=0.7$ and reduced pressure is $P\sigma^3/\epsilon=4$. Full circles, $N=108$; shaded circles, $N=600$; and open circles, $N=1008$. (b) Initial configuration is ct structure. Reduced temperature is $kT/\epsilon=0.9$ and reduced pressure is $P\sigma^3/\epsilon=28$. Full circles, $N=108$; shaded circles, $N=500$; and open circles, $N=1008$. (c) Initial configuration is hex structure. Reduced temperature is $kT/\epsilon=1$ and reduced pressure is $P\sigma^3/\epsilon=50$. Full circles, $N=108$; shaded circles, $N=512$; and open circles, $N=1000$.

bcc, ct, or hex phase in each case; however, the different symmetries of these phases make it unlikely that the system may arrange particles into a single homogeneous phase, and after very long runs (longer than the 2×10^6 MC steps shown in Figs. 9 and 10) one could expect at most a configuration with different coexisting crystalline domains of the same symmetry. Configuration snapshots (not shown) also corroborate that the fcc is unstable at the above state points. One can draw the same conclusion when simulations are performed at constant volume (*NVT* simulations). In this case the system seems to evolve to the other structures, and the instability is observed very rapidly in the simulation (first few MC steps). Again it is unlikely that the system may reach homogeneous bcc, ct, and hex phases, even after very long simulations. The second series of simulations consisted of three *NPT* simulations. The system was started in each case with configurations corresponding to bcc, ct, and hex phases. In each case we performed simulations with different numbers of particles: 108, 600, and 1008 for the bcc structure, 108, 500, and 1008 for the ct structure, and 125, 512,

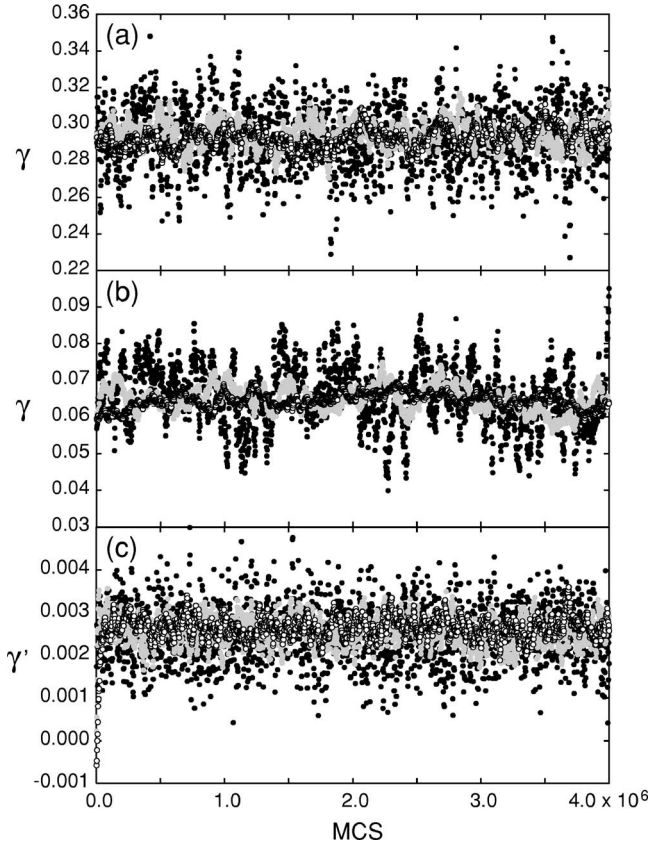


FIG. 12. Evolution of the order parameters γ and γ' with MC steps (MCS), plotted every 4000 steps, for an *NPT* simulation of the square-well model with $\delta=0.43\sigma$. See Fig. 11 for key to symbols.

and 1000 for the hex structure. In each run for each phase we constructed the initial configuration at the density obtained from the (approximate) averaged density estimated from the previous simulation with the smallest (108 or 125, depending on the phase) number of particles. In order to make it easier for the system to find an equilibrium structure possibly different from the initial one (bcc, ct, or hex), we allowed the box side lengths *and* their orientations to fluctuate and, in addition, we conducted very long runs (4×10^6 MC steps). Results for the evolution of the reduced energy per particle and the order parameter γ with respect to MC steps are shown in Figs. 11 and 12 (data points are plotted every 4000 steps). In Fig. 13 we present the angular-averaged distribution functions. Table I shows the averaged values and the standard deviations for the energy and order parameter obtained over the last 3.9×10^4 MC steps. In all cases, since the initial conditions are close to typical equilibrium configurations, the equilibration period cannot be visualized in the figures, with the exception of the order parameter in the case of the hex phase. The angular-averaged distribution functions obtained from simulations with different system sizes are practically indistinguishable from each other in the bcc and hex phases; they differ by a very small amount in the case of the ct phase. The maximum difference (3%) occurs at contact and at $r=\sigma+\delta$ for the ct structure with $N=108$ particles; in the remaining points the difference decreases to $\sim 0.1\%$. For other numbers of particles and/or structures the difference is

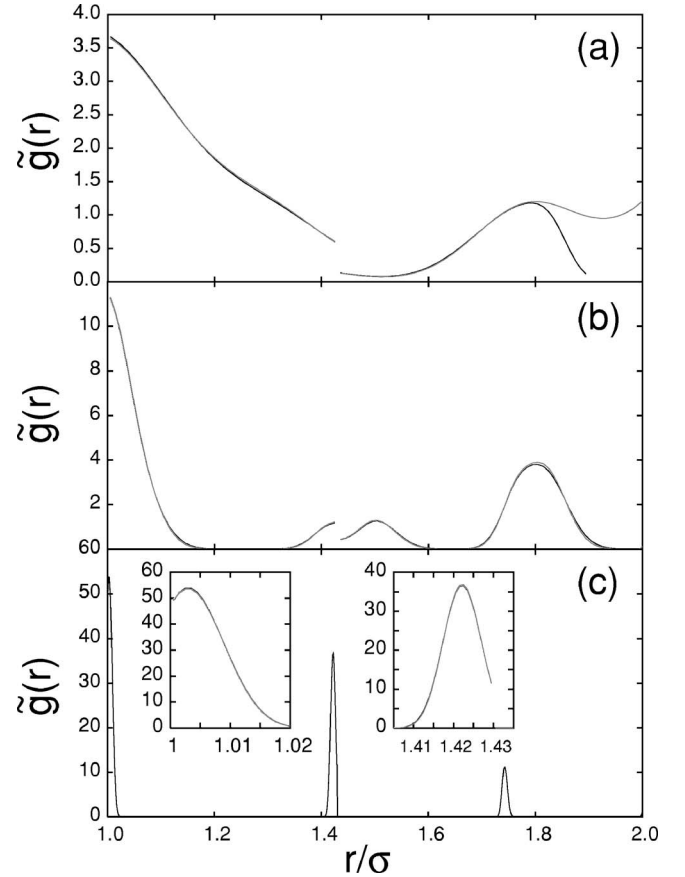


FIG. 13. Angular-averaged distribution functions $\tilde{g}(r)$ for the square-well model with $\delta=0.43\sigma$ as obtained by *NPT* simulation for the same values of N , reduced temperature, and reduced pressure as those in Figs. 11 and 12 (for key to lines see captions of these figures). (a) bcc structure, (b) ct structure, and (c) hex structure. In (c) insets show detail of the first two peaks. Dark line (a), representing the corresponding function for the bcc structure and $N=108$ particles, departs from the rest of the lines for $r \geq 1.8\sigma$ due to the simulation box being too small to contain that range of radial distance.

TABLE I. Results of *NPT* simulations. For each phase and number of particles used, the averaged reduced energy per particle $\langle E/N\epsilon \rangle$ with variance σ_E and the averaged order parameter $\langle \gamma \rangle$ or $\langle \gamma' \rangle$ (the latter for the hex phase) with variance σ_γ are given.

Phase	N	$\langle E/N\epsilon \rangle$	σ_E	$\langle \gamma \rangle$ or $\langle \gamma' \rangle$	σ_γ
bcc	108	-6.861590	0.038389	0.292469	0.016537
bcc	600	-6.867411	0.015723	0.294235	0.006961
bcc	1008	-6.868453	0.012038	0.292718	0.005465
ct	108	-6.889486	0.043789	0.065675	0.008412
ct	500	-6.887017	0.020063	0.064744	0.003385
ct	1008	-6.889486	0.012451	0.064541	0.001941
hex	125	-9.999984	0.000225	0.002490	0.000656
hex	512	-9.999985	0.000106	0.002565	0.000319
hex	1000	-9.999985	0.000075	0.002654	0.000228

always less than 1%. The averaged reduced energy and order parameter are also very weakly dependent on the system size (see Table I). Note that, as expected, the fluctuations of these variables clearly depend on system size. Note also that the density range of stability of the hex(20) phase is very small and very near close-packing conditions, which explains why the averaged reduced energy per particle is practically equal to -10 and the corresponding fluctuations are asymmetric.

As a final remark, we note that in order to obtain reliable averaged values $(0.5-1) \times 10^5$ MC steps are sufficient in all cases, save the energy and order parameter for the ct phase. In this case averaging over this range of steps leads to deviations from values obtained from much longer runs of less than 2%, which is enough for our aims. For the purpose of obtaining accurate angular-averaged distribution functions the above number of steps is again enough in all cases.

-
- [1] J. A. Baxter and D. Henderson, *Rev. Mod. Phys.* **48**, 587 (1976); J. P. Hansen and I. R. McDonald, *The Theory of Simple Liquids* (Academic, London, 1990).
- [2] M. Lisal and I. Nezbeda, *Mol. Phys.* **96**, 335 (1999); Y. Y. Duan, L. Shi, L. Q. Sun, M. S. Zhu, and L. Z. Han, *Int. J. Thermophys.* **21**, 393 (2000).
- [3] C. J. Peng, H. L. Liu, and Y. Hu, *Chin. J. Chem.* **19**, 1165 (2001).
- [4] K. Rah and B. C. Eu, *J. Chem. Phys.* **116**, 7967 (2002).
- [5] A. Skibinsky, S. V. Buldyrev, A. Scala, S. Havlin, and H. E. Stanley, *Phys. Rev. E* **60**, 2664 (1999).
- [6] E. Zaccarelli, G. Foffi, K. A. Dawson, F. Sciortino, and P. Tartaglia, *Phys. Rev. E* **63**, 031501 (2001); W. Gotze and M. Sperl, *J. Phys.: Condens. Matter* **15**, S869 (2003).
- [7] L. A. Del Pino, A. L. Benavides, and A. Gil-Villegas, *Mol. Simul.* **29**, 345 (2003); S. Q. Zhou, *J. Phys. Chem. B* **107**, 3585 (2003).
- [8] V. N. Ryzhov and E. E. Tareyeva, *Physica A* **314**, 396 (2002).
- [9] A. J. White, *J. Chem. Phys.* **113**, 1580 (2000).
- [10] I. Kusaka, *J. Chem. Phys.* **118**, 5510 (2003).
- [11] H. Sakai, F. H. Stillinger, and S. Torquato, *J. Chem. Phys.* **117**, 297 (2002).
- [12] Y. X. Yu, M. H. Han, and G. H. Gao, *Phys. Chem. Chem. Phys.* **3**, 437 (2001); G. Foffi, K. A. Dawson, S. V. Buldyrev, F. Sciortino, E. Zaccarelli, and P. Tartaglia, *Phys. Rev. E* **65**, 050802(R) (2002).
- [13] K. Shukla and R. Rajagopalan, *Mol. Phys.* **81**, 1093 (1994).
- [14] B. H. Chang and Y. C. Bae, *Biomacromolecules* **4**, 1713 (2003); J. J. Grigsby, H. W. Blanch, and J. M. Prausnitz, *Biophys. Chem.* **91**, 231 (2001); K. Murakami, *Langmuir* **15**, 4270 (1999).
- [15] S. Saadeddine, J. F. Wax, B. Grosdidier, J. G. Gasser, C. Regnaut, and J. M. Dubois, *Phys. Chem. Liq.* **28**, 221 (1994); J. N. Nzali and W. Hoyer, *Z. Naturforsch., A: Phys. Sci.* **55**, 381 (2000).
- [16] G. T. Evans, *J. Chem. Phys.* **115**, 1440 (2001); B. Cernuschi-Frias, H. J. Gonzalez, and F. Cernuschi, *Mol. Phys.* **49**, 505 (1998).
- [17] D. A. Young and B. J. Alder, *J. Chem. Phys.* **70**, 473 (1979); P. C. Hemmer and G. Stell, *Phys. Rev. Lett.* **24**, 1284 (1970).
- [18] P. Bolhuis and D. Frenkel, *Phys. Rev. Lett.* **72**, 2211 (1994); P. Bolhuis, M. Hagen, and D. Frenkel, *Phys. Rev. E* **50**, 4880 (1994).
- [19] A. Daanoun, C. F. Tejero, and M. Baus, *Phys. Rev. E* **50**, 2913 (1994); C. N. Likos, Zs. T. Németh, and H. Löwen, *J. Phys.: Condens. Matter* **6**, 10965 (1994); C. Rascón, G. Navascués, and L. Mederos, *Phys. Rev. B* **51**, 14899 (1995).
- [20] D. A. Young, *J. Chem. Phys.* **58**, 1647 (1973).
- [21] D. A. Young and B. J. Alder, *J. Chem. Phys.* **73**, 2430 (1980).
- [22] C. N. Likos, *Phys. Rep.* **348**, 267 (2001).
- [23] Note that for one-component systems the three thermodynamic free-energy surfaces corresponding to three different phases can cross at one point, giving rise to a triple point. It is theoretically possible that this point be on the free-energy surface of a fourth phase, which would generate a quadruple point. This situation can only be realized for an artificially constructed interparticle potential, and the Gibbs phase rule excludes this possibility in the general case.
- [24] Since the particle distribution around a lattice site is not sharp but smeared out.
- [25] This can also be considered as a hexagonal phase with a two-site basis.
- [26] E. Velasco, L. Mederos, and G. Navascués, *Mol. Phys.* **97**, 1273 (2001).
- [27] C. Rascón, L. Mederos, and G. Navascués, *Phys. Rev. E* **54**, 1261 (1996).
- [28] C. Rascón, L. Mederos, and G. Navascués, *Phys. Rev. Lett.* **77**, 2249 (1996).
- [29] J.-P. Hansen and I. R. McDonald, *Theory of Simple Liquids* (Academic, New York, 1986).
- [30] L. Verlet and J. J. Weis, *Phys. Rev. A* **5**, 939 (1972).
- [31] L. Mederos, G. Navascués, and E. Velasco, *Phys. Rev. E* **65**, 016131 (1999).
- [32] At densities close to packing the structure has 20 neighbors within the potential well: six nearest neighbors, two next-nearest neighbors, and 12 next-next-nearest neighbors. The relatively large number of particles within the interaction range compensates for the very small entropy of this configuration.
- [33] This is based on estimates on the location of next-nearest neighbors and selected computer simulations.